Supporting Information

Barr et al. 10.1073/pnas.1305923110

SI Materials and Methods

Mucus Sample Collection. Mucus samples were collected directly from the surface of organisms using a syringe, swab, or custom suction device. Environmental samples were collected as close to the mucus sample as possible, typically within 30–50 cm of the mucosal surface. Specific organism details are as follows:

Sea anemones were sampled from tidal rock pools at Ocean Beach, San Diego, CA. Surface mucus was collected by a custom suction device that dislodges surface mucus using a stream of 0.02 μm filtered seawater; the environmentalg sample was seawater collected directly above the anemone.

Hard corals were sampled at the Birch Aquarium, San Diego, CA. Surface mucus was collected by syringe directly from coral surfaces; environmental water samples were collected directly above the coral.

The polychaete, along with surrounding water, was collected at Scripps Pier, San Diego, CA, and carefully transported to the laboratory in a container. Surface mucus was collected via syringe, and the environmental sample was seawater from the container.

Teleost surface mucus was sampled at the Birch Aquarium, San Diego, CA. Surface mucus was collected by custom suction device; the environmental water sample was collected directly above the teleost within its tank.

Human gum mucus was sampled from a male subject with no current pathology/disease. Surface mucus was collected by swab; the environmental sample was expectorated saliva. Consent was obtained for all human samples collected under the San Diego State University Institutional Review Board #2121.

Mouse intestine was excised from a healthy mouse. Surface mucus was collected by cutting open the intestine, washing the mucosal surface with 0.02 μm-filtered PBS buffer, then scraping off the mucus layer; the environmental sample was collected from the intestinal lumen directly adjacent to the sampled mucosa. All animal experiments were approved by the Committee on the Use and Care of Animals (SDSU, APF #10-08-024D) and performed using accepted veterinary standards.

Bacterial and Phage Counts from Mucus and Environmental Samples. Samples of mucus and the adjacent environment were collected directly from nine evolutionarily diverse mucosal surfaces (Fig. S1). Samples were transported and maintained on ice until processed. All samples were fixed overnight in 0.5% glutaraldehyde at 4 °C, then incubated in 6.5 mM DTT at 37 °C for 1 h to assist mucus degradation. A 1–100-μL aliquot was diluted with 2 mL of 0.02 μm SM buffer (100 mM NaCl, 8 mM $MgSO_4$, 50 mM Tris·Cl, in dH_2O), briefly mixed, then filtered onto a 0.02-μm Anodisc polycarbonate filter (Whatman). Filters were stained with 10× SYBR Gold, washed, and visualized on a Zeiss epifluorescence microscope. For each sample, 20–30 images were taken for both bacteria and virus-like particles. Images were analyzed using Image-Pro Plus 5.1 software (MediaCybernetics). Counts of bacteria and virus-like particles (referred to as "phage" throughout the text) per milliliter were made as previously described (1).

Tissue Culture Cells and Mucus Reduction. Monolayers of various mucus-producing and non–mucus-producing tissue culture (TC) cells were grown to confluence in six-well Multiwell tissue culture plates (Becton Dickinson). (*i*) Mucus-producing TC cells were exposed to 1 μg/mL of a phorbol ester, phorbol-12-myristate 13-acetate (Sigma–Aldrich) in the culture media overnight to stimulate the mucin secretory response (2). (*ii*) The mucolytic agent *N*-acetyl-L-cysteine (NAC; Sigma–Aldrich) was used to chemically remove mucus from A549 TC cells (60 mM NAC in serum-free media for 1 h with agitation) (3). Mucus depletion was confirmed using periodic acid-Schiff–Alcian blue (PAS/AB) (Fig. S2). (*iii*) A mucus-knockdown (*MUC*$^-$) A549 cell line was produced by transduction of A549 cells with GIPZ Lentiviral Human MUC1 shRNA and TRIPZ Inducible Lentiviral Human MUC5AC shRNA as target vectors; an *shControl* A549 cell line was produced using the GIPZ Nonsilencing Lentiviral shRNA Control as a control vector (Thermo Scientific). Knockdown of mucus production in the *MUC*$^-$ cell line was confirmed by Western blot analysis and PAS/AB (Sigma–Aldrich; Figs. S3 and S4).

Transfection and Selection of A549 TC Mucus-Negative Clones. A549 cells were transduced with GIPZ Lentiviral Human MUC1 shRNA and TRIPZ Inducible Lentiviral Human MUC5AC shRNA as target vectors or GIPZ Nonsilencing Lentiviral shRNA Control as a control vector (Thermo Scientific) according to the manufacturer's instructions. Viral particles were produced by transfecting HEK 293T cells with a combination of plasmids containing 2 μg of packaging vector pCMV d8.2 containing the gag-pol proteins of HIV-1, 3 μg of the transfer vectors containing the LTRs of HIV-1, 3 μg of vesicular stomatitis virus envelope glycoprotein plasmid, and 1.5 μg of pci-HIV-1 viral protein R accessory protein plasmid. Growth medium was replaced 24 h post transfection, and viral supernatant was collected 48 and 72 h after transfection and then filtered through 0.45-μm polytetrafluoroethylene (PTFE) filters (Pall Corporation). A549 cells were seeded into six-well culture plates and grown to ∼70% confluence. The cells then were washed twice in serum-free media before being incubated overnight in 1 mL of growth media and 1 mL of virus-containing media containing 5 μg/mL of polybrene. The transduced cells subsequently were washed and cultured for 24 h in complete medium with 2 μg/mL of doxycycline to induce expression of shRNA. Cells then were sorted using a BD FACSAria (BD Biosciences) at the San Diego State University Flow Cytometry Facility. A 100-μm nozzle was used at a sheath pressure of 20 psi. Excitation source was a 488-nm laser and emissions were collected using 530/30 band pass (BP) and 585/42 BP filters for GFP and red fluorescent protein, respectively. Between 10,000 and 300,000 cells were sorted for each population and collected in a 5-mL tube with 250 μL of FBS. The efficiency of MUC1-MUC5AC knockdown was confirmed by Western blot analysis and PAS/AB (Sigma–Aldrich), a stain for mucus-like substances.

Western Blot Analysis. Expression of MUC1 (a membrane-tethered mucin) and MUC5AC (a secreted gel-forming mucin) was examined by Western blot analysis. *MUC–*, *shControl*, and native A549 cell lines were grown to confluence and then lysed using radio-immunoprecipitation assay (RIPA) buffer (Thermo Scientific) containing 2 mM Na_3VO_4, 100 mM NaF, 10 mM sodium pyrophosphate, 1 mM PMSF, and protease inhibitor mixture (Millipore). Aliquots containing 50 μg of total protein were subjected to SDS/PAGE, and the protein bands were transferred to a polyvinylidene difluoride membrane (Sigma–Aldrich). Membranes were blocked with 5% nonfat milk in Tris-buffered saline containing 0.05% Tween 20 at room temperature for 1 h and then incubated overnight at 4 °C with mouse anti-human MUC1 monoclonal antibody (clone S.854.6; Thermo Scientific), mouse anti-human MUC5AC monoclonal antibody (clone 2H7; Sigma–Aldrich), and rabbit anti-human GAPDH antibody (Millipore). After three washes, membranes were incubated for 1 h at room

temperature with anti-mouse or anti-rabbit IgG horseradish peroxidase-linked, species-specific, whole antibody (Fisher Scientific). Immunoreactivity was visualized and band intensity was normalized to the constitutively expressed GAPDH protein.

Multiple Particle Tracking. Assays were performed in plastic well chambers mounted on glass slides that had been coated with poly (dimethylsiloxane) to prevent phage adherence. Five microliters of 10^9 mL^{-1} SYBR Gold-labeled phage suspensions was added to 50 μL of 1% (wt/vol) mucin solution in 1× PBS buffer. Trajectories of fluorescently labeled phage were observed using a DeltaVision Spectris Model DV4 deconvolution microscope (Applied Precision) equipped with a 100× Olympus PlanApo 1.4 lens. Movies were captured using SoftWoRx 5.0.0 (Applied Precision): 100-ms temporal resolution for 30 s, 10 analyses per sample, $n > 100$ particle trajectories per analysis. Trajectories were analyzed with the ParticleTracker plugin for ImageJ (4). The coordinates of phage particle centroids were transformed into time-averaged mean square displacements: $\langle \Delta r^2(\tau) \rangle = \langle \Delta x^2 + \Delta y^2 \rangle$, from which effective diffusivities ($\langle D_{eff} \rangle$) were calculated; $D_{eff} = \langle \Delta r^2(\tau) \rangle / (4\ \tau)$ (5, 6).

Glycan Microarray. Phage binding to glycans was assayed using printed mammalian glycan microarrays (version 5.1, Consortium for Functional Glycomics Core) containing 610 glycan targets. Samples of highly antigenic outer capsid protein (hoc^+) T4 phage, hoc^- T4 phage, and buffer controls were applied to separate glycan microarray slides. Each slide received 35 μL of sample, 35 μL of binding buffer (Tris saline with 2 mM Ca^{2+}, 2 mM Mg^{2+}, 1% bovine serum albumin (BSA), and 0.05% Tween 20), and a coverslip. Slides first were incubated for 1 h at room temperature and washed with binding buffer. Slides then were incubated in SYBR Gold fluorescence dye (diluted 1:10,000 in binding buffer) for 1 h under a coverslip at room temperature, washed, dried, and immediately scanned in a PerkinElmer ProScanArray microarray scanner using an excitation wavelength of 488 nm. ImaGene software (BioDiscovery, Inc) was used to quantify fluorescence. Normalized relative fluorescence unit (RFU) values reported are the average (after subtraction of background buffer fluorescence) from six spots for each glycan represented on the array.

Phylogenetic Analysis of Ig-Like Domains. The SEED database (www.theseed.org) collection of Ig-like polycystic kidney disease (PKD) protein families (Pfam) (PF00801) and the T4 Hoc sequence were searched against the 124 viral metagenomic datasets contained in the My Metagenome (MyMg) database (http://edwards.sdsu.edu/cgi-bin/mymgdb/show.cgi) using tBLASTn (PubMed accession numbers: 16336043, 17620602, 19156205, 19816605, 20547834, 17921274, 18441115, 19892985, 19555373, 20573248, 20631792, 21167942.79, 21193730.87, 21219518.96, 21245307.04, 21271095.12, 21296883.2, 21322671.29, 21348459.37, 21374247.45, 21400035.53; MG-Rast IDs: 21167942.79, 21193730.87, 21219518.96, 21245307.04, 21271095.12, 21296883.2, 21322671.29, 21348459.37, 21374247.45, 21400035.53).

Sequences with an e value of less than 1e-5 to Ig-like domains were retrieved. ORFs were called from the metagenome reads using Artemis (Wellcome Trust Sanger Institute); their position in the FASTA file is shown in Table S2. ORFs that were 60 bp long with 40% tBLASTn identity to T4 Hoc or a member of the PKD Ig Pfam were retained. The six contigs containing Ig-like hypervariable domains from the published study by Minot et al. (7) were downloaded from the National Center for Biotechnology Information (NCBI). Identical sequences were collapsed using the Trie clustering method implemented in Qiime (8). The resulting unique sequences were mapped to the position-specific scoring matrix for the PKD Ig Pfam (PF00801) using hmmalign (9). The hmmalign trimming function was used; sequences that were dominated by gaps after alignment were removed. A maximum likelihood tree was generated from the aligned unique sequences using FastTree version 2.1.1 SSE3 and viewed in MEGA 5. Environmental data for the metagenomes were obtained from the MyMg database. In a separate analysis, structural homology of these same sequences to a carbohydrate-binding protein (10) was determined using the Phyre2 structural homology prediction pipeline (www.sbg.bio.ic.ac.uk/phyre2/html/help.cgi).

1. Patel A, et al. (2007) Virus and prokaryote enumeration from planktonic aquatic environments by epifluorescence microscopy with SYBR Green I. *Nat Protoc* 2(2):269–276.
2. Forstner G, Zhang Y, McCool D, Forstner J (1993) Mucin secretion by T84 cells: Stimulation by PKC, Ca2+, and a protein kinase activated by Ca2+ ionophore. *Am J Physiol* 264(6 Pt 1):G1096–G1102.
3. Alemka A, et al. (2010) Probiotic colonization of the adherent mucus layer of HT29MTXE12 cells attenuates Campylobacter jejuni virulence properties. *Infect Immun* 78(6):2812–2822.
4. Sbalzarini IF, Koumoutsakos P (2005) Feature point tracking and trajectory analysis for video imaging in cell biology. *J Struct Biol* 151(2):182–195.
5. Suh J, Dawson M, Hanes J (2005) Real-time multiple-particle tracking: Applications to drug and gene delivery. *Adv Drug Deliv Rev* 57(1):63–78.
6. Lai SK, et al. (2007) Rapid transport of large polymeric nanoparticles in fresh undiluted human mucus. *Proc Natl Acad Sci USA* 104(5):1482–1487.
7. Minot S, Grunberg S, Wu GD, Lewis JD, Bushman FD (2012) Hypervariable loci in the human gut virome. *Proc Natl Acad Sci USA* 109(10):3962–3966.
8. Caporaso JG, et al. (2010) QIIME allows analysis of high-throughput community sequencing data. *Nat Methods* 7(5):335–336.
9. Eddy SR (2009) A new generation of homology search tools based on probabilistic inference. *Genome Inform* 23(1):205–211.
10. Najmudin S, et al. (2006) Xyloglucan is recognized by carbohydrate-binding modules that interact with β-glucan chains. *J Biol Chem* 281(13):8815–8828.

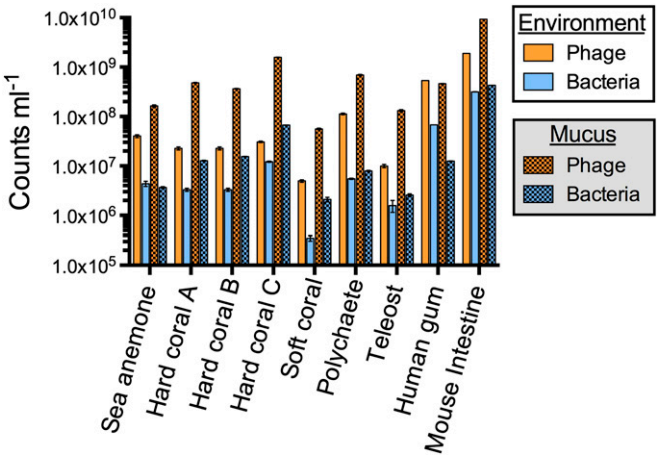

Fig. S1. Epifluorescence counts of phage and bacteria from diverse environments and mucosa. (Left to right) Invertebrates: *Actiniaria* sp., *Acropora* sp., *Echinopora* sp., *Oxypora* sp., *Capnela* sp., and *Phyllodoce* sp. Vertebrates: *Paralichthys* sp., *Homo sapiens*, and *Mus musculis*. Error bars represent ±SD with $n > 25$.

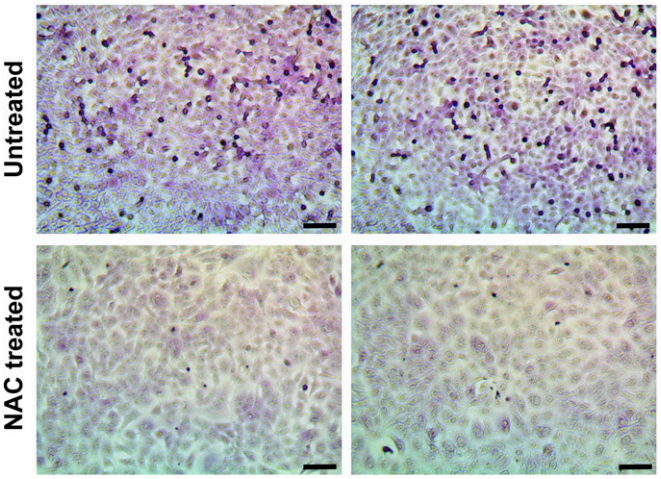

Fig. S2. Mucolytic treatment of mucus-producing A549 cells. Mucus removal from A549 lung epithelial cells by NAC treatment was assessed by PAS/AB stain, which stains mucus-like substances pink/purple. Scale bars represent 100 μm.

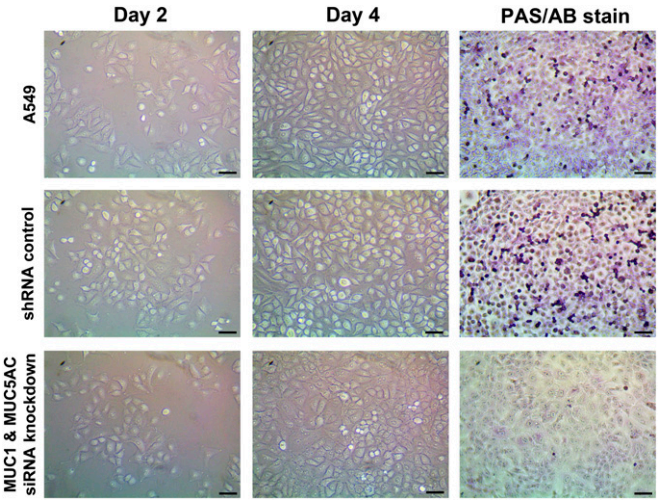

Fig. S3. Growth and mucus production of A549 and siRNA knockdown cell lines. Shown are mucus-producing A549 lung epithelial TC cells, mucus-producing nonsense shRNA control A549 cell line (*shControl*), and non–mucus-producing *MUC1* and *MUC5AC* shRNA knockdown A549 cell line (*MUC*$^{-}$) after 2 and 4 d in culture. Mucus production was assessed on day 5 by PAS/AB stain, which stains mucus-like substances pink/purple. Scale bars represent 100 μm.

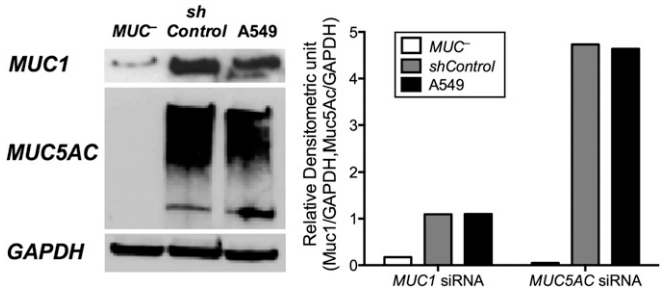

Fig. S4. Western blot analysis of MUC1 and MUC5AC in total cell lysates of A549 lung epithelial cell knockdowns. Lysates of confluent cell layers were separated by SDS/PAGE and then immunoblotted with anti-MUC1 and anti-MUC5AC antibodies. Shown are the *MUC*⁻ knockdown cell line, the nonsilencing *shControl* control cell line, and native A549 cells. GAPDH was used as an intracellular protein control.

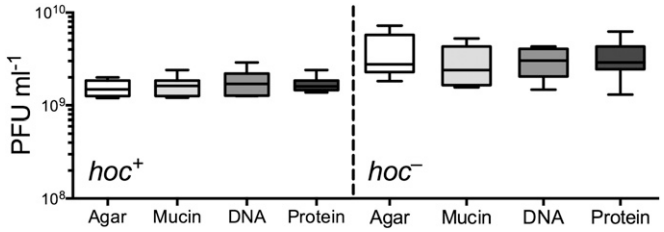

Fig. S5. Surface-free control for the assay of phage adherence to mucus-associated macromolecules. Both *hoc*⁺ and *hoc*⁻ T4 phage (10^9 pfu·mL^{-1}) were serially diluted to 1×10^{-7} and 1×10^{-8}, and then incubated in 1% (wt/vol) solutions of mucin, DNA, or protein in 1 mL LB for 30 min at 37 °C. Each incubation mixture was then mixed with *Escherichia coli* top agar and layered over plain agar plates. Resulting plaque-forming unit (PFU) counts showed that infectivity of *hoc*⁺ and *hoc*⁻ T4 phage was not significantly altered in the presence of the macromolecules used in the phage adherence assays (mucin, DNA, and BSA protein).

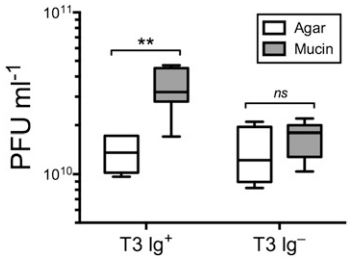

Fig. S6. Adherence of Ig$^+$ and Ig$^-$ T3 phage to mucin. Phage adherence assays to mucin-coated agar plates were performed as described in *SI Materials and Methods*, except that the Ig$^+$ and Ig$^-$ T3 phage (10^{11} pfu·mL^{-1}) were serially diluted to 1×10^{-9} and 1×10^{-10} pfu·ml^{-1}. The resultant PFU counts of adherent phage showed that Ig$^+$ T3 phage adhered to mucin-coated agar plates significantly more than to the plain agar control plates ($n = 6$, $t = 4.443$, $^{**}P = 0.0012$, unpaired t test), whereas there was no significant increase in adherence for the Ig$^-$ T3 phage. *ns*, not significant.

Table S1. Phyre2 structural homology of Ig-like proteins encoded by viral metagenomes

		Phyre2 analysis			ORF, bp				
No.	Environment	PDB ID	Confidence, %	Identity, %	Start	Stop	Length	Database	Sequence identifier
1	Sputum	2C26-A	99.8	29	29	277	248	MyMg	d7c74d66ea493c0c1fca41f718d22125_16271_279
2	Sputum	2C26-A	99.9	36	280	555	275	MyMg	d7c74d66ea493c0c1fca41f718d22125_64742_278
3	Sputum	2C26-A	99.7	32	837	1,066	229	MyMg	03ca0e6ad90102ab264cf521ed58209e_112029_232
4	Sputum	2C26-A	99.7	26	2,951	3,184	233	MyMg	03ca0e6ad90102ab264cf521ed58209e_52923_234
5	Sputum	2C26-A	99.7	32	3,417	3,654	237	MyMg	2da3ea31d1b30a11b0f080a5b91b9df2_256934_240
6	Sputum	2C26-A	99.7	31	4,189	4,416	227	MyMg	03ca0e6ad90102ab264cf521ed58209e_134692_228
7	Freshwater	2C26-A	99.8	29	3,935	4,188	253	MyMg	6f8c77f72920950139dc6b3520cf86b7_69438_254
8	Oral	2C26-A	99.8	29	2,437	2,715	278	MyMg	f44d959b723905a049b0334f19668e5c_48421_279
9	Sputum	2C26-A	99.8	30	2,716	2,949	233	MyMg	875f11dbd745609c9d3e12c5b3b5636a_66237_235
10	Sputum	2C26-A	99.9	30	16,236	16,491	255	MyMg	88f61453e560016a0e2a238351d7292b_109758_257
11	Sputum	2C26-A	99.9	29	15,508	15,766	258	MyMg	ebdf0605a03616ab168eddf68ca506e1_121095_259
12	Marine*	1E07-A	99.8	13	3	800	797	MyMg	05d2b5884d248d570fe8a2c0d390c97c_3911_800
13	Human feces	2C26-A	88.8	23	1	246	245	MyMg	f58fff76a10b642883986ee0e1a30514_10941_246
14	Human feces	2C26-A	94.7	31	248	484	236	MyMg	f58fff76a10b642883986ee0e1a30514_22104_238
15	Human feces	2C26-A	86.8	22	720	960	240	MyMg	f58fff76a10b642883986ee0e1a30514_10554_243
16	Human feces	2C26-A	86	29	1,445	1,682	237	MyMg	f58fff76a10b642883986ee0e1a30514_32210_238
17	Human feces	2C26-A	85.5	32	2,400	2,637	237	MyMg	f58fff76a10b642883986ee0e1a30514_22379_238
18	Human feces	2C26-A	90.1	26	3,122	3,361	239	MyMg	f58fff76a10b642883986ee0e1a30514_6620_240
19	Human feces	2C26-A	98.1	11			574	NCBI	gi 377806168 gb AFB75876.1
20	Human feces	2C26-A	99	15			429	NCBI	gi 377806248 gb AFB75953.1
21	Human feces	2C26-A	99.6	18			529	NCBI	gi 377806350 gb AFB76049.1

All Ig-like domain homologs shown in Fig. 4*A* displayed high structural homology with a promiscuous carbohydrate-binding domain [Protein Data Bank (PDB) 2C26]. The Hoc homolog from a marine sample (no. 12, column 1) displayed high structural homology with 1E07-A as well as several other immune proteins. bp, base pairs. *Hoc homolog.

Table S2. Glycan microarray analysis of T4 and *hoc*⁻ phage displayed in Fig. 4*A*

Glycan no.	Structure	Linkage	T4 RFU	T4 %CV	*hoc*⁻ RFU	*hoc*⁻ %CV
609	GlcNAcb1-3Fuca	-N(CH3)-O-(CH2)2-NH2	4,921	3	394	16
610	Galb1-3GalNAcb1-4(Neu5Aca2-8Neu5Aca2-8Neu5Aca2-3) Galb1-4Glcb	-N(CH3)-O-(CH2)2-NH2	4,685	11	472	13
573	Neu5Aca2-8Neu5Aca2-3Galb1-3GalNAcb1-4(Neu5Aca2-3) Galb1-4Glc	-N(CH3)-O-(CH2)2-NH2	4,161	1	316	11
608	Neu5Aca2-6Galb1-4GlcNAcb1-3Galb1-4GlcNAcb1-2Mana1-6(Neu5Aca2-6Galb1-4GlcNAcb1-3Galb1-4GlcNAcb1-2Mana1-3)Manb1-4GlcNAcb1-4GlcNAcb	Asparagine	4,685	4	497	17
145	Galb1-3GalNAcb1-4Galb1-4Glcb	CH2CH2CH2NH2	5,823	3	565	7
195	Glca1-4Glcb	CH2CH2CH2NH2	5,845	1	544	3
514	GalNAcb1-4(6S)GlcNAc	CH2CH2CH2NH2	4,518	6	568	17
287	Neu5Gca	CH2CH2CH2NH2	4,182	3	356	9
119	Gala1-4(Fuca1-2)Galb1-4GlcNAcb	CH2CH2CH2NH2	4,157	3	331	8
336	GalNAca1-3(Fuca1-2)Galb1-4GlcNAcb1-3Galb1-4GlcNAcb1-3Galb1-4GlcNAcb	CH2CH2NH2	7,670	31	472	51
217	Manb1-4GlcNAcb	CH2CH2NH2	4,766	3	647	24
144	Galb1-3GalNAcb1-4(Neu5Aca2-3)Galb1-4Glcb	CH2CH2NH2	4,797	4	589	26
517	Galb1-4(6P)GlcNAcb	CH2CH2NH2	4,751	11	526	20
218	Neu5Aca2-3Galb1-4GlcNAcb1-3Galb1-4(Fuca1-3)GlcNAcb	CH2CH2NH2	4,737	3	322	10
334	GalNAcb1-3Gala1-4Galb1-4GlcNAcb1-3Galb1-4Glcb	CH2CH2NH2	4,261	4	499	8
143	Galb1-3GalNAcb1-3Gala1-4Galb1-4Glcb	CH2CH2NH2	4,236	1	451	13
581	Galb1-4GlcNAcb1-3Galb1-4GlcNAcb1-3Galb1-4GlcNAcb1-3Galb1-4GlcNAcb1-3Galb1-4GlcNAcb1-2Mana1-6(Galb1-4GlcNAcb1-3Galb1-4GlcNAcb1-3Galb1-4GlcNAcb1-3Galb1-4GlcNAcb1-3Galb1-4GlcNAcb1-2Mana1-3) Manb1-4GlcNAcb1-4(Fuca1-6)GlcNAcb	EN or NK	5,465	6	262	7
360	Fuca1-2Galb1-3GlcNAcb1-2Mana1-6(Fuca1-2Galb1-3GlcNAcb1-2Mana1-3)Manb1-4GlcNAcb1-4GlcNAcb	GENR	4,914	2	482	12
588	Galb1-4GlcNAcb1-3Galb1-4GlcNAcb1-3Galb1-4GlcNAcb1-3Galb1-4GlcNAcb1-3Galb1-4GlcNAcb1-6(Galb1-4GlcNAcb1-3Galb1-4GlcNAcb1-3Galb1-4GlcNAcb1-3Galb1-4GlcNAcb1-3Galb1-4GlcNAb1-2)Mana1-6(Galb1-4GlcNAcb1-3Galb1-4GlcNAcb1-3Galb1-4GlcNAcb1-3Galb1-4GlcNAcb1-3Galb1-4GlcNAcb1-2Mana1-3) Manb1-4GlcNAcb1-4(Fuca1-6)GlcNAcb	KVANKT	3,926	2	154	5
470	Glca1-4Glca1-4Glca1-4Glcb	NHCOCH2NH	7,521	10	1,288	17
516	(4S)GalNAcb	NHCOCH2NH	6,148	2	464	3
359	KDNa2-3Galb1-3GalNAca	**Threonine (O-linked glycan)**	7,484	17	1,080	24
471	Neu5Aca2-3Galb1-4GlcNAcb1-6(Neu5Aca2-3Galb1-4GlcNAcb1-3)GalNAca	**Threonine (O-linked glycan)**	5,877	6	585	2
491	Neu5Aca2-3Galb1-3GlcNAcb1-6GalNAca	**Threonine (O-linked glycan)**	4,755	2	394	8
596	Neu5Aca2-3Galb1-4GlcNAcb1-3Galb1-4GlcNAcb1-6 (Neu5Aca2-3Galb1-4GlcNAcb1-3Galb1-4GlcNAcb1-3) GalNAca	**Threonine (O-linked glycan)**	4,703	14	242	7
595	GlcNAcb1-3Galb1-4GlcNAcb1-6(GlcNAcb1-3Galb1-4GlcNAcb1-3)GalNAca	**Threonine (O-linked glycan)**	4,653	1	392	9
605	Neu5Aca2-6Galb1-4GlcNAcb1-3Galb1-4GlcNAcb1-6 (Neu5Aca2-6Galb1-4GlcNAcb1-3Galb1-4GlcNAcb1-3) GalNAca	**Threonine (O-linked glycan)**	4,078	1	410	10
480	Neu5Aca2-6Galb1-4GlcNAcb1-6GalNAca	**Threonine (O-linked glycan)**	4,143	5	301	20
592	Neu5Aca2-3Galb1-4GlcNAcb1-3Galb1-4GlcNAcb1-3GalNAca	**Threonine (O-linked glycan)**	4,200	11	266	11

"Glycan no." indicates the glycan ID number used on the Consortium for Functional Glycomics Version 5.1 microarray. "Linkage" denotes the chemical linkage joining the glycan to the macromolecule. Bold threonine linkages represent O-linked glycan residues likely to be associated with mucin glycoproteins.